eFood

WILEY

RESEARCH ARTICLE OPEN ACCESS

Pulsed Electric Field Processing Enhances the Endothelial Bioefficacy of Red Beet (*Beta vulgaris* L.) Extracts by Restoring Endothelial Nitric Oxide Synthase–Nitric Oxide Signaling in High-Fat Diet Rats

Eunju Jang[1] | Tae-Baek Lee[1] | Lisa Tonini[1] | Soobin Choi[1] | YoonA Jeon[2] | Taehyun Kim[2] | Taeyoung Kang[2] | Hyuk-Joon Choi[3] | Changhwan Ahn[1,2]

[1]Laboratory of Veterinary Physiology, College of Veterinary Medicine, Jeju National University, Jeju, Republic of Korea | [2]College of Veterinary Medicine and Veterinary Medical Research Institute, Jeju National University, Jeju, Republic of Korea | [3]BKbio, Jeju, Republic of Korea

Correspondence: Changhwan Ahn (cahn@jejunu.ac.kr)

Received: 16 February 2026 | **Revised:** 12 May 2026 | **Accepted:** 2 June 2026

Funding: Ministry of Small and Medium-sized Enterprises (SMEs) and (MSS), Grant/Award Number: S3404552; Korea Technology and Information Promotion Agency for SMEs (TIPA)

Keywords: *Beta vulgaris* L. | endothelial dysfunction | high-fat diet | nitric oxide | pulsed electric field

ABSTRACT

Endothelial dysfunction is a central mechanism underlying the development of major cardiovascular diseases, including hypertension and atherosclerosis. Red beet (*Beta vulgaris* L.)–derived products are widely recognized as functional dietary components that support metabolic and vascular health, and multiple extraction strategies have been explored to optimize their biological efficacy. Pulsed electric field (PEF) processing has emerged as a nonthermal approach capable of enhancing the recovery of plant-derived bioactive compounds by increasing cellular permeability, while avoiding thermal degradation. However, the influence of PEF processing on endothelial-specific outcomes, including NO bioavailability, vascular remodeling, and endothelium-dependent function, has not been systematically investigated. In this study, we examined whether PEF processing qualitatively alters the vascular bioefficacy of red beet extracts in a high-fat diet–induced model of endothelial dysfunction. PEF-treated extracts restored endothelial signaling and improved vascular functional responsiveness to a greater extent than conventionally extracted preparations. Our findings demonstrate that PEF-treated red beet extracts exert superior protective effects on endothelial function compared with non-PEF–treated preparations. These results indicate that processing technology itself represents a biologically relevant determinant of vascular efficacy and highlight the potential of PEF-based approaches to enhance the endothelial benefits of plant-derived functional ingredients.

1 | Introduction

Endothelial cells form a monolayer at the interface between blood and vascular tissues, constituting the vascular endothelium. These cells play crucial roles in regulating vascular tone through balanced vasodilation and vasoconstriction, hemostasis and thrombosis, and inflammatory responses to maintain circulatory homeostasis. Specifically, endothelial dysfunction is a key mechanism underlying the development of major cardiovascular diseases including hypertension, atherosclerosis, and diabetes. This dysfunction is marked by an imbalance between the production of vasoprotective mediators, such as nitric oxide (NO), and elevated oxidative stress driven by enzymes such as NADPH oxidase (Higashi 2022).

A high-fat diet (HFD) is a well-established driver of endothelial dysfunction, primarily through impairment of the AMPK–PI3K–Akt–eNOS signaling pathway in the aorta, which is essential for

This is an open access article under the terms of the Creative Commons Attribution License, which permits use, distribution and reproduction in any medium, provided the original work is properly cited.

© 2026 The Author(s). *eFood* published by John Wiley & Sons Australia, Ltd. on behalf of International Association of Dietetic Nutrition and Safety.

Summary

- Red beet extracts restore endothelial NO signaling and vascular function in HFD rats.
- PEF pretreatment enhances the vascular efficacy of beet extracts beyond ethanolic extraction.
- Processing technology emerges as a biologically relevant determinant of endothelial outcomes.

maintaining endothelial homeostasis (García-Prieto et al. 2015). In Sprague–Dawley rats, moderate HFD feeding induces progressive body weight gain accompanied by cardiometabolic complications, including hypertension (Dobrian et al. 2000). At the vascular level, reduced AMPK activity in endothelial cells of obese rats is closely associated with lipid accumulation, increased apoptosis, and diminished NO production, collectively impairing endothelium-dependent vasorelaxation. Based on this evidence, an HFD-induced endothelial dysfunction model was selected to evaluate the ameliorative effects of *Beta vulgaris L.* extract in the present study.

Red beets contain high amounts of water-soluble betalains, dietary fiber, carotenoids, minerals, vitamins, and saponins (Milton-Laskibar et al. 2021). In human studies, red beet juice has been extensively studied and reported to exert a variety of biological activities, including antioxidant (Darvish et al. 2024) and anti-inflammatory effects (Fejes et al. 2024), as well as anti-obesity properties (Litwin et al. 2019). These findings support the potential of red beet–derived products as functional dietary components for metabolic and vascular health. Although the vascular benefits of beet-derived products are well recognized, the influence of extraction processing conditions on the biological quality of the resulting extracts remains poorly characterized.

To improve the recovery of bioactive compounds from plant materials, pulsed electric field (PEF) technology has emerged as a promising nonthermal processing approach. PEF processing enhances plant bioactive recovery through electroporation-mediated cell membrane permeabilization, effectively increasing pigment extractability from beetroot while minimizing thermal degradation (Fincan et al. 2004). Systematic optimization of PEF parameters—including field strength, pulse number, and duration—has been shown to further improve betanin yield (López et al. 2009; Luengo et al. 2016). While the PEF process is well recognized for improving extraction efficiency through increased cellular permeability, its impact on endothelial-specific outcomes, including NO bioavailability, vascular remodeling, and endothelium-dependent vascular function, has not yet been systematically evaluated.

While accumulating evidence supports the ability of red beet and beet juice consumption to reduce blood pressure and improve vascular function through increased NO bioavailability via nitrate metabolism and antioxidant activity, the specific contribution of endothelial NO production and the detailed signaling modulation of endothelial nitric oxide synthase (eNOS) to the vascular protective effects of red beet extracts remains insufficiently elucidated. Given the central role of endothelial NO in vascular homeostasis, reduced endothelial NO bioavailability impairs vasodilatory capacity and promotes atherogenic processes, including platelet aggregation, leukocyte adhesion and migration. Therefore, this study aimed to determine whether the PEF process qualitatively alters the vascular bioefficacy of beet extracts, focusing on eNOS signaling, vascular structural remodeling, and endothelium-dependent functional recovery in an HFD-induced model of endothelial dysfunction.

2 | Materials and Methods

2.1 | Preparation of Red Beet Extracts and Pulsed Electric Field Pretreatment

All red beet (*B. vulgaris* L. var. Udan) extracts were prepared from samples harvested in August and provided by BKbio (Jeju, Republic of Korea). The extracts were classified as Beetvaso or Beetvaso-P according to the extraction process. For the preparation of Beetvaso, raw materials were washed, ground and then extracted with 50% ethanol at 55°C for 4 h. After extraction, the samples were filtered, the solvent was removed by rotary evaporation, and the extracts were dried to a powder. For the preparation of Beetvaso-P, raw materials were subjected to PEF pretreatment prior to the extraction process. The beetroot was pretreated with PEF (HVP-5, Elea, Quakenbrück, Germany) at 2.0 kV/cm, 20 μs, 50 Hz, and 500 pulses, based on conditions previously reported to effectively enhance cell membrane permeabilization in vegetable matrices (Kim et al. 2024). Following PEF pretreatment, the materials were extracted using the same procedure as for Beetvaso. The extraction and PEF pretreatment procedures are summarized in Figure 1A.

2.2 | Animals and Experimental Design

All animal experiments were approved by the Institutional Animal Care and Use Committee of Jeju National University (Jeju, Republic of Korea; Approval No. 2022-0055). Rats were housed under controlled environmental conditions (temperature 22 ± 2°C, relative humidity 50%–60%, 12 h light/12 h dark cycle) with ad libitum access to standard chow and water throughout the experimental period. A HFD (TD.06414) was purchased from Inotiv (West Lafayette, IN, USA) and provided 60% of total caloric intake from fat. Male Sprague–Dawley rats (7 weeks old, 250–270 g) were acclimatized for 1 week under standard laboratory conditions before the start of the experiment. Following the acclimation period, rats were fed either a normal chow diet or a 60% HFD for 3 months. Following 3 months of dietary intervention, rats continued their respective diets and were randomly assigned to eight experimental groups ($n = 8$/group) as follows:

Group 1: Normal chow diet + 0.9% NaCl (CON).

Group 2: 60% HFD + 0.9% NaCl.

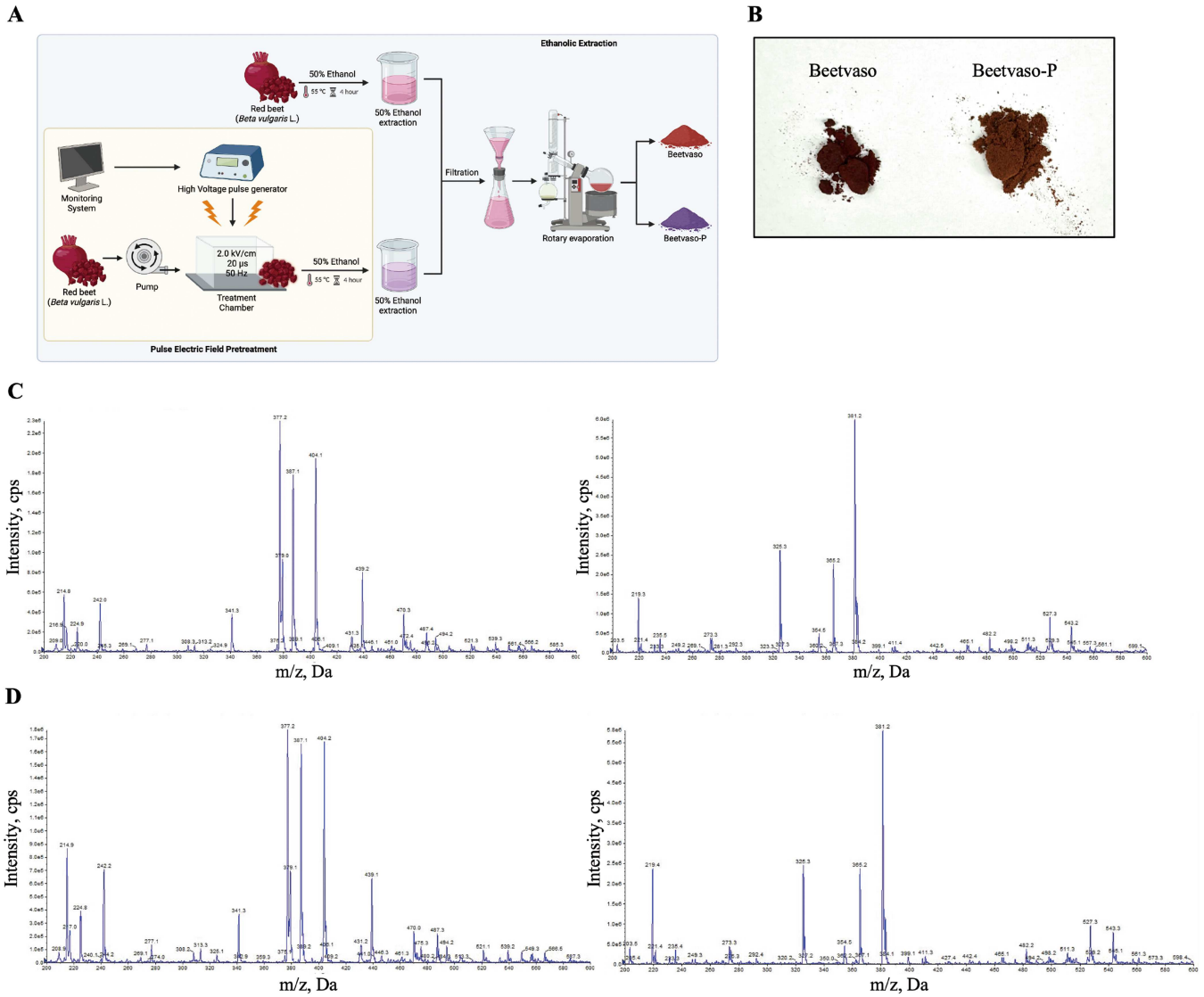
Group 3: 60% HFD + Beetvaso 50 mg/kg.

Group 4: 60% HFD + Beetvaso 100 mg/kg.

Group 5: 60% HFD + Beetvaso 200 mg/kg.

Group 6: 60% HFD + Beetvaso-P 50 mg/kg.

Group 7: 60% HFD + Beetvaso-P 100 mg/kg.



E

		Intensity, cps	
		Beetvaso	Beetvaso-P
Betacyanin	Betanidin	1780300	1662300
	Betanin	99689	undetected
Betaxanthin	Vulgaxanthin I	1945600	1677000
	Indicaxanthin	5982600	5811800
	Glutamine-betaxanthin	334030	317790

FIGURE 1 | PEF-induced differences in betalain pigment composition between Beetvaso and Beetvaso-P. (A) Schematic illustration of the red beet extraction procedures for Beetvaso and Beetvaso-P. The schematic illustration was created using BioRender (BioRender.com). (B) Appearance of the two beetroot extracts. Lyophilized powders of Beetvaso and Beetvaso-P were placed on white background to illustrate the marked color difference. (C) Representative LC-ESI-MS spectra (m/z 200–600) of the Beetvaso acquired in negative (left) and positive (right) ionization modes. (D) Representative LC-ESI-MS spectra of the Beetvaso-P acquired in negative (left) and positive (right) ionization modes. (E) Summary table showing relative peak intensities of representative betacyanin (betanin, betanidin) and betaxanthin (vulgaxanthin I, indicaxanthin, glutamine-betaxanthin) pigments in Beetvaso and Beetvaso-P. These spectral profiles indicate that, under the present conditions, PEF processing was associated with the selective loss of betanin while betaxanthins are largely preserved, consistent with the observed color shift from red to yellow and the distinct vascular effects of Beetvaso-P.

Group 8: 60% HFD + Beetvaso-P 200 mg/kg.

Beetvaso and Beetvaso-P were administered orally once daily for 3 weeks. Body weight was measured daily throughout the experimental period. At the end of the treatment period, rats were deeply anesthetized with isoflurane, and blood was collected by cardiac puncture until exsanguination was confirmed, after which the aorta was carefully isolated and stored at −50°C until further analysis.

2.3 | Blood Pressure Measurement

Systolic and diastolic blood pressure were measured non-invasively using the tail-cuff method. Prior to measurement, rats were placed in restrainers and allowed to acclimate for approximately 30 min to minimize stress-induced variability. Blood pressure measurements were performed using a Kent CODA 8 Blood Pressure Monitor System (Kent Scientific Corporation, Torrington, CT, USA) equipped with Volume Pressure Recording (VPR) sensor technology, allowing non-invasive assessment of systolic and diastolic blood pressure. For each measurement, an occlusion cuff was first positioned at the base of the tail, followed by placement of a VPR cuff distal to the occlusion cuff. All measurements were conducted under identical conditions according to the manufacturer's instructions, and environmental variables were carefully controlled to reduce stress during the procedure. Blood pressure data were collected and recorded in real time using the CODA system software.

2.4 | Assessment of Coagulation Parameters (PT and aPTT)

To assess coagulation function, additional blood samples were collected into citrate-containing tubes. Plasma was obtained by centrifugation of the blood samples, and prothrombin time (PT) and activated partial thromboplastin time (aPTT) were measured using an automated coagulation analyzer (CG02N, A&T Corporation, Tokyo, Japan) according to the manufacturer's protocol.

2.5 | Enzyme-Linked Immunosorbent Assay (ELISA)

Blood samples were collected into tubes containing citrate buffer to prevent coagulation. Plasma was obtained by centrifugation and used directly for analysis without dilution. Plasma levels of vascular cell adhesion molecule-1 (VCAM-1) were measured using ELISA kits (Bioswamp, RA20552). Plasma concentrations of von Willebrand factor (vWF), plasminogen activator inhibitor-1 (PAI-1), intercellular adhesion molecule-1 (ICAM-1), P-selectin, and E-selectin were determined using ELISA kits (Elabscience; vWF, E-EL-R1079; PAI-1, E-EL-R3058; ICAM-1, E-EL-R2850; P-selectin, E-EL-R3045; E-selectin, E-EL-R0893). All assays were performed in accordance with the manufacturers' protocols. Absorbance was measured at 450 nm using an Epoch Microplate Spectrophotometer (BioTek, Agilent, Santa Clara, CA, USA).

2.6 | Biochemical Analysis

Plasma levels of total cholesterol (TC), triglyceride (TG), and LDL-cholesterol (LDL-C) were measured using a quantification kit (Solarbio; TC, BC1985; TG, BC0625; LDL-C, BC5335) according to the manufacturer's protocol. TC, TG, and LDL-C levels were measured spectrophotometrically at 500 nm, 420 nm, and 546 nm, respectively, using the Epoch Microplate Spectrophotometer described above.

2.7 | Histological Analysis and ImageJ-Based Morphometric Quantification

Aortic rings were excised, rinsed in cold PBS, and fixed in 4% PFA (24–48 h, room temperature). Samples were paraffin-embedded using graded ethanol dehydration, xylene clearing, and paraffin infiltration, then sectioned at 3–5 μm. Sections were deparaffinized, rehydrated, stained with Mayer's hematoxylin (Dako; S3309) and eosin Y solution (318906-500 ML), dehydrated, cleared, and coverslipped. Images were acquired using a ZEISS Lattice SIM 3 in transmitted-light mode. Morphometric analyses were performed in ImageJ (v1.53t, NIH, USA) after spatial calibration. Areas were quantified by manual ROI tracing, and thickness was measured with perpendicular line segments at multiple evenly spaced positions per section, averaged per animal. Aortic lumen/IEL/EEL boundaries were used to compute lumen and EEL metrics, wall thickness indices, and normalized ratios.

2.8 | Measurement of Nitric Oxide (NO) Levels in Rat Aorta

To quantify intracellular NO production in rat aortic tissue, a NO-sensitive fluorescent probe, diamino-fluorescein-2 diacetate (DAF-2DA, Abcam, Cambridge, UK), was used. Immediately after sacrifice, the thoracic aorta was carefully excised and cut into thin cross-sections. The sections were incubated with DAF-2DA (10 μM) at 37°C for 30 min in the dark to minimize NO degradation (Toque et al. 2017). Following incubation, the sections were gently rinsed with phosphate-buffered saline to remove excess dye. DAF-2DA–derived fluorescence was promptly visualized using a Leica DMi8 fluorescence microscope (Leica Microsystems, Wetzlar, Germany) at 10× and 20× magnification, using a FITC filter cube (Ex. 480/40, DC. 505LP, Em. 527/30; #11525307). Fluorescence intensity was quantified using ImageJ software (NIH, Bethesda, MD, USA), and the mean fluorescence intensity per field was calculated and normalized to the control group.

2.9 | Analysis of Vascular Function

Aortic rings were rapidly excised from the descending aorta, carefully sectioned into segments (3–4 mm in length), and immersed in Krebs buffer. The rings were then suspended in organ baths aerated with 95% O_2/5% CO_2 and filled with modified Krebs buffer as previously described (Kaya et al. 2003). Changes in isometric tension were recorded using a force-displacement transducer (FT-03E, sensitivity: 5–20 mV/g; Grass Instruments, Quincy, MA, USA) connected to a PowerLab data acquisition system (PowerLab 8/35, AD Instruments, Medford, MA, USA) and stored digitally for analysis. Each aortic ring was equilibrated under a resting tension of 2.0 g for 30 min, during which the Krebs buffer was replaced every 15 min. After the equilibration period, aortic rings were precontracted with phenylephrine (PE, 1 μM). Once a stable contraction plateau was achieved, cumulative concentrations of acetylcholine (ACh; 10^{-8}–10^{-5} M) were added to assess endothelium-dependent relaxation. Endothelium-independent relaxation was evaluated by the addition of sodium nitroprusside (SNP; 10^{-5} M). To minimize channel-specific bias, Beetvaso and Beetvaso-P

treatments were alternately applied across organ bath channels, ensuring that no single channel was continuously exposed to the same extract throughout the experiment.

2.10 | Human Umbilical Vein Endothelial Cells (HUVEC) Culture and Tube Formation Assay

To complement the in vivo vascular findings, HUVECs were used as an in vitro endothelial model to directly assess the endothelial protective effects of Beetvaso and Beetvaso-P under inflammatory conditions. HUVECs were purchased from Thermo Fisher Scientific (C0035C) and cultured in Human Large Vessel Endothelial Cell Basal Medium (formerly Medium 200; M200500) supplemented with Low Serum Growth Supplement (LSGS; S00310) and fetal bovine serum (FBS, Gibco) at a final concentration of 10%. Cells were maintained in a humidified incubator at 37°C with 5% CO_2, and the culture medium was replaced every 2 days.

For the tube formation assay, 96-well plates were precoated with Matrigel (Corning, 356231; 50 μL/well) and allowed to polymerize at 37°C for 30 min. HUVECs were seeded at a density of 2×10^4 cells per well to assess the effects of Beetvaso and Beetvaso-P extracts on TNF-α-induced inhibition of angiogenic tube formation. Cells were incubated with tumor necrosis factor-α (TNF-α, 20 ng/mL) alone or in combination with Beetvaso or Beetvaso-P extracts (0.01% or 0.1%). After 4 h of incubation, capillary-like structures formed by the cells were observed and imaged using a Leica DMi8 microscope. Tube formation was quantified by measuring junction number, mesh number, and total tube length using the Angiogenesis Analyzer plugin in ImageJ (NIH, USA) (Zhou et al. 2020). All experiments were performed using cells between passages 3 and 6 to ensure experimental consistency.

2.11 | RNA Isolation and Real-Time Quantitative PCR

Total RNA was extracted using TRIzol reagent (Invitrogen, Thermo Fisher Scientific, USA) according to the manufacturer's protocol. The concentration and quality of the RNA were measured using an Epoch Microplate Spectrophotometer (BioTek, Agilent, Santa Clara, CA, USA). Subsequently, 1 μg of total RNA was used to generate the first-strand cDNA using M-MLV Reverse Transcriptase (Invitrogen, 28025013) with random primers (Promega, C1181). qRT-PCR was performed with the QuantStudio 1 Real-Time PCR system (Applied Biosystems, USA) using PowerUp SYBR Green PCR Master Mix (Applied Biosystems, A25742, USA). Expression levels of genes associated with pro-inflammatory endothelial activation (*Ccl2, Nox2, Mmp9, Vcam1, Nfkb1, Icam1*) and endothelial-protective homeostasis (*Nos3, Klf2, Abca1, Adipoq*) were normalized to β-actin using the ΔΔCt method. Primer sequences are listed in Table 1.

TABLE 1 | List of primer sequences used for quantitative real-time PCR.

Gene	Category		Primer Sequence (5′→3′)	T_m (°C)	Size (bp)	Efficiency (%)
Actb	Reference	Forward	CCTCTGAACCCTAAGGCCAAC	62.0	134	100.9
		Reverse	GTCGTACCACTGGCATTGTGATG	63.0		
Ccl2	Pro-inflammatory	Forward	CTACAAGAGAATCACCAGCAGCAG	62.5	136	97.4
		Reverse	CCAATAAGGAATGGGTCCAGAAGTAC	62.2		
Nox2	Pro-inflammatory	Forward	GCATCCATATCCGTATTGTGGGAG	62.3	124	96.2
		Reverse	GTGTTCAGCTATGAGGTGGTGATG	62.5		
Mmp9	Pro-inflammatory	Forward	CAGTACTCTACCTGTACCGGCGAG	64.0	127	101.6
		Reverse	GCCATGCGCTGGGCTTAGATC	66.8		
Vcam1	Pro-inflammatory	Forward	GTCAGCAGTCAAATGGAGTCTGAAC	62.9	132	102.8
		Reverse	GTGAACCTGACCTGCTCAAGTGATG	64.9		
Nfkb1	Pro-inflammatory	Forward	GGCTGGAGAAGATGAGGGAGTAGTGC	64.7	127	94.6
		Reverse	GACAGAAGACACGAGGCTGCAACTC	63.8		
Icam1	Pro-inflammatory	Forward	GTCTCCGAGGTCAGGCAGC	64.3	132	98.0
		Reverse	GTGTTCCCTGGAAGGCCTGTTTC	65.2		
Nos3	Homeostasis	Forward	GGAGTCCAGCGAACAGCAGG	64.9	130	100.4
		Reverse	GGTACTACTCTGTCAGCTCAGCAC	63.7		
Klf2	Homeostasis	Forward	CACCAACTGCGGCAAGACCTAC	65.3	134	96.5
		Reverse	GAAGCCTTATCATTGCAACTGGGAC	64.7		
Abca1	Homeostasis	Forward	CGGTGACAAGCAGAGCTGTCTG	65.0	130	101.1
		Reverse	CAGACCTGCTCAGCGGGATG	64.7		
Adipoq	Homeostasis	Forward	CAGGATATCCTGGTCACAATGGGATAC	63.8	129	92.4
		Reverse	CAGGAGATGCTGGAATGACAGGAG	64.1		

2.12 | Targeted Gene Bioinformatics Data Analysis Processing

Gene expression data were analyzed in R. Log_2 fold changes relative to the control group were calculated for each endpoint, and group-wise comparisons were performed using two-sided Welch's *t*-tests with Benjamini–Hochberg FDR correction (adjusted $p < 0.05$). Heatmaps, principal component analysis (PCA), volcano plots, and pathway enrichment were generated using ComplexHeatmap, ggplot2, and gprofiler2, respectively.

2.13 | Protein Purification and Western Blot

Rat aorta and HUVECs were lysed in RIPA lysis buffer (Thermo Fisher Scientific, USA). A total of 20 μg of protein per sample was loaded onto 7.5% SDS-PAGE gels and transferred to membranes. The membranes were blocked with 5% BSA in TBS-T for 1 h at room temperature and then incubated overnight at 4°C with primary antibodies against eNOS (PA1-037, Invitrogen), phospho-eNOS (Ser1177; PA5-104858, Invitrogen), phospho-eNOS (Thr495; PA5-104859, Invitrogen), and β-actin (MA5-15739, Invitrogen). The target protein bands were quantified via densitometry using ImageJ software (v1.53t, NIH, USA). The relative protein levels were determined by normalizing each band to its β-actin control.

2.14 | Statistical Analysis

Data were expressed as the mean ± SD. Statistical significance was assessed using one-way ANOVA with Dunnett's post hoc test for multiple comparisons when appropriate. All statistical analyses were conducted using GraphPad Prism version 10 (GraphPad Software, San Diego, CA, USA). $p < 0.05$ was considered statistically significant.

3 | Results

3.1 | PEF-Induced Remodeling of Betalain Composition in Beetvaso-P

To characterize PEF-induced changes in pigment composition, we first compared the betalain profiles of Beetvaso and Beetvaso-P. Visual inspection of the lyophilized powders revealed a marked color shift from deep red in Beetvaso to yellowish tones in Beetvaso-P, suggesting alterations in the relative abundance of betacyanins and betaxanthins (Figure 1B). Consistent with this, LC-ESI-MS spectra recorded in both negative and positive ionization modes showed distinct m/z patterns between Beetvaso and Beetvaso-P, supporting the presence of PEF-induced alterations in the underlying pigment profile (Figure 1C,D). LC-ESI-MS analysis confirmed this impression, showing a pronounced reduction of the major betacyanin betanin in Beetvaso-P, while levels of betanidin and representative betaxanthins (vulgaxanthin I, indicaxanthin, and glutamine-betaxanthin) were largely preserved under the applied PEF conditions (Figure 1E). This PEF-driven compositional shift from a betanin-rich to a relatively betaxanthin-enriched profile provides a basis to hypothesize that qualitative differences in betalain speciation, rather than total pigment content alone, may influence the vascular effects of Beetvaso versus Beetvaso-P in subsequent in vivo studies.

3.2 | Effects of Beetvaso and Beetvaso-P on Systolic Blood Pressure and Coagulation Parameters

Since HFD-associated cardiometabolic risk involves dyslipidemia, hypertension, and prothrombotic changes, we assessed the impact of Beetvaso and Beetvaso-P on hemodynamic and coagulation parameters. Figure 2A presents an overview of the in vivo experimental design. During the 3-week oral administration period, body weight remained relatively stable in both the CON and HFD control groups. In contrast, rats treated with Beetvaso or Beetvaso-P exhibited an overall trend toward body weight reduction, suggesting a modest attenuation of HFD-associated weight gain (Figure 2B).

Consistent with the development of HFD-induced vascular stress, systolic and diastolic blood pressure were elevated in the HFD group, rising approximately 1.42- and 1.59-fold above CON levels, respectively. Oral administration of Beetvaso or Beetvaso-P dose-dependently attenuated these elevations, with the greatest reductions observed at 200 mg/kg for both extracts. Diastolic pressure normalized to CON-comparable levels across all Beetvaso-P doses, and the lowest systolic blood pressure was recorded in the Beetvaso-P 200 mg/kg group (Figure 2C,D). HFD also induced marked dysregulation of plasma lipid profiles, with TC, TG, and LDL-C elevated approximately 1.4-, 1.6-, and 2.5-fold above CON levels, respectively. Both extracts dose-dependently improved TC, TG, and LDL-C, but only Beetvaso-P normalized all three parameters, restoring LDL-C to CON-comparable levels at all doses (Figure S1).

To determine whether these improvements extended to coagulation balance, we next examined coagulation-related parameters. After 3 months of HFD feeding, PT remained unchanged relative to CON, whereas aPTT was significantly decreased (0.66-fold), reflecting a shift toward a hypercoagulable state within the intrinsic pathway. Both Beetvaso and Beetvaso-P significantly restored aPTT toward CON-comparable levels (Figure 2E,F), indicating correction of HFD-induced intrinsic pathway abnormalities.

Plasma levels of vWF and PAI-1 were then measured by ELISA. vWF was elevated approximately 2.0-fold above CON in the HFD group. Beetvaso dose-dependently reduced vWF toward CON-comparable levels, whereas Beetvaso-P showed no significant effect (Figure 2G). Conversely, PAI-1 was elevated approximately 1.8-fold in the HFD group relative to CON, indicating suppressed fibrinolytic activity. Beetvaso-P restored PAI-1 to CON-comparable levels across all doses, whereas Beetvaso showed less consistent reduction (Figure 2H). These complementary patterns suggest distinct antithrombotic mechanisms, with Beetvaso primarily attenuating endothelial vWF release and Beetvaso-P preferentially suppressing fibrinolytic inhibition through PAI-1 reduction.

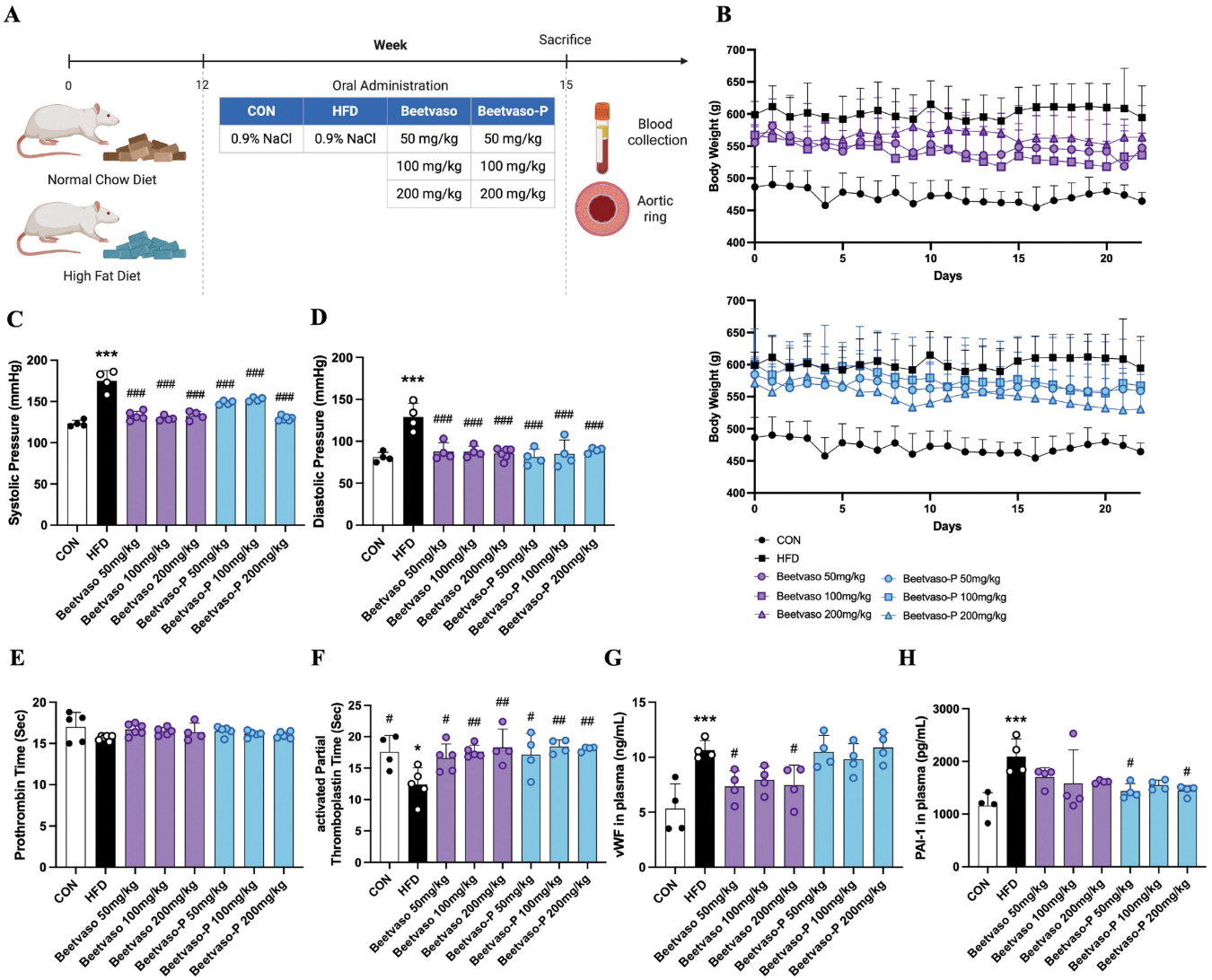


FIGURE 2 | Effects of Beetvaso and Beetvaso-P on body weight, blood pressure, and coagulation parameters in HFD-fed rats. Rats were fed an HFD for 3 months, followed by oral administration of Beetvaso or Beetvaso-P for 3 weeks. (A) Schematic illustration of the in vivo experimental design. (B) Body weight profiles during the oral administration period of Beetvaso or Beetvaso-P (50, 100, and 200 mg/kg). (C) Systolic blood pressure and (D) Diastolic blood pressure measured by the tail-cuff method. (E) Prothrombin time (PT). (F) Activated partial thromboplastin time (aPTT). (G) Plasma levels of von Willebrand factor (vWF) and (H) plasminogen activator inhibitor-1 (PAI-1). Schematic illustrations were created using BioRender (BioRender.com). Data are presented as mean ± SD. Statistical significance is indicated as $^{*}p < 0.05$, $^{***}p < 0.001$ vs. CON; $^{\#}p < 0.05$, $^{\#\#}p < 0.01$, $^{\#\#\#}p < 0.001$ vs. HFD, as annotated in the graphs ($n = 4$). Statistical graphs were generated using GraphPad Prism version 10.

3.3 | Beetvaso and Beetvaso-P Attenuate HFD-Induced Aortic Wall Remodeling

To determine whether Beetvaso or Beetvaso-P can ameliorate HFD-induced aortic remodeling, we quantified morphometric parameters in aortic cross-sections. Figure 3A depicts the anatomical partitioning used for morphometry, subdividing the aortic wall into the intima, media, and adventitia and Figure 3B shows representative H&E-stained aortic sections from each group.

Under HFD conditions, lumen area was reduced approximately 0.87-fold relative to CON, whereas total wall thickness, IMT, intima thickness, and media thickness were increased approximately 1.61-, 1.56-, 1.82-, and 1.47-fold, respectively, consistent with inward remodeling (Figure 3C–G). Restoration of lumen area was specific to Beetvaso-P; Beetvaso did not significantly increase lumen area at any dose, whereas Beetvaso-P at 200 mg/kg restored lumen area to CON-comparable levels (Figure 3C). Both extracts dose-dependently reduced HFD-induced aortic wall thickening across all morphometric parameters. Beetvaso produced partial attenuation of total wall thickness, IMT, intima thickness, and media thickness, improving these measures relative to HFD but not fully restoring them to CON-comparable levels. However, Beetvaso-P consistently outperformed Beetvaso, with total wall thickness and media thickness reaching CON-comparable levels at 200 mg/kg, and intima thickness normalized below CON at the same dose. IMT was most effectively reduced by Beetvaso-P at 200 mg/kg, approaching control values (Figure 3D–G).

To assess whether remodeling occurred within a fixed outer vessel boundary and luminal preservation, we quantified the

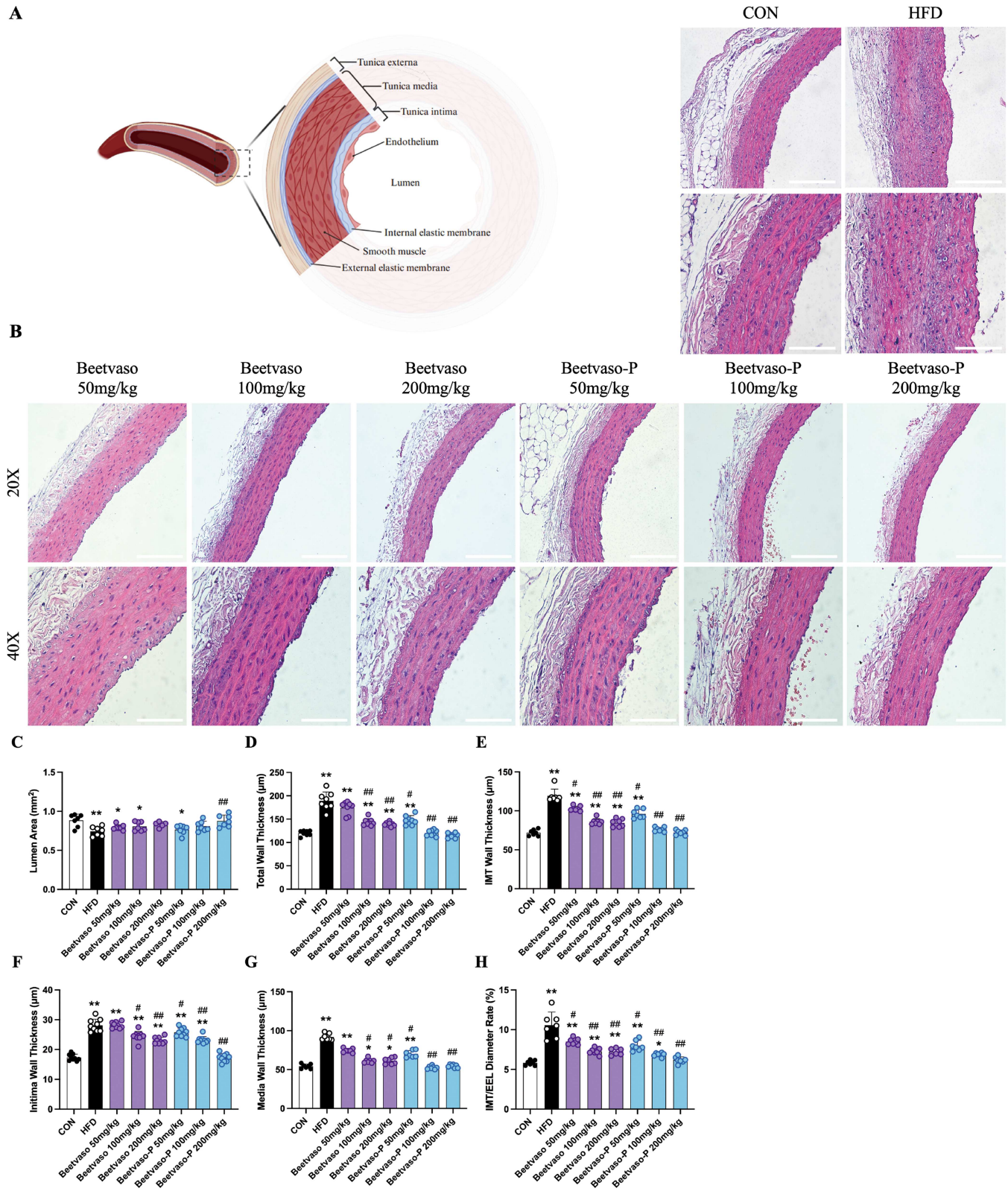


FIGURE 3 | Beetvaso and Beetvaso-P attenuate HFD-induced aortic wall remodeling. (A) Schematic representation of aortic wall compartmentalization for morphometric analysis, including lumen, intima, media, adventitia, and intima–media thickness (IMT). The schematic illustration was created using BioRender (BioRender.com). (B) Representative hematoxylin and eosin (H&E)–stained transverse sections of thoracic aorta from CON, HFD, and HFD-fed rats treated with Beetvaso or Beetvaso-P (50, 100, or 200 mg/kg). Scale bars: 100 μm (low magnification) and 50 μm (high magnification). Quantitative morphometric analyses include (C) lumen area, (D) total wall thickness, (E) intima–media thickness (IMT), (F) intima thickness, (G) media thickness, and (H) IMT/EEL diameter ratio, where EEL denotes the external elastic lamina. Statistical significance is indicated as $^{*}p < 0.05$, $^{**}p < 0.01$, vs. CON; $^{\#}p < 0.05$, $^{\#\#}p < 0.01$ vs. HFD, as annotated in the graphs ($n = 8$). Statistical graphs were generated using GraphPad Prism version 10.

IMT/EEL diameter ratio, EEL area and diameter, and the lumen/EEL area ratio (Figure 3H and Figure S2). IMT/EEL was increased by HFD and reduced by both extracts, with Beetvaso-P at 200 mg/kg showing the greatest normalization toward control levels (Figure 3H). EEL area and EEL-derived diameter did not differ among groups (Figure S2B,C). Within this unchanged EEL boundary, HFD reduced the lumen/EEL area ratio, whereas Beetvaso-P at 100 and 200 mg/kg significantly increased this ratio, indicating improved luminal preservation (Figure S2D).

Overall, both extracts attenuated HFD-induced inward aortic remodeling by reducing wall thickening and improving luminal preservation within an unchanged EEL-defined vessel boundary. Beetvaso-P exhibited the most consistent dose-dependent effects, with the 200 mg/kg dose providing the strongest normalization of wall metrics and lumen-related indices.

3.4 | Effects of Beetvaso and Beetvaso-P on Endothelial Activation and Vascular Inflammation

To assess endothelial activation, we evaluated VCAM-1 and ICAM-1, representative endothelial adhesion molecules that are markedly upregulated under inflammatory conditions. P-selectin and E-selectin were also measured as additional markers of endothelial activation.

Plasma levels of soluble VCAM-1 were elevated approximately 1.5-fold in the HFD group relative to CON; both Beetvaso and Beetvaso-P reduced VCAM-1 to CON-comparable levels across all doses (Figure 4A). Soluble ICAM-1 was more markedly elevated, reaching approximately 5-fold above CON levels under HFD. Beetvaso dose-dependently reduced ICAM-1, with the 200 mg/kg dose restoring CON-comparable levels, whereas Beetvaso-P produced significant but comparatively less consistent reductions (Figure 4A). Consistently, E-selectin was elevated approximately 4.0-fold and P-selectin approximately 1.8-fold above CON in the HFD group. Both extracts significantly attenuated E-selectin and P-selectin levels across all doses, with Beetvaso showing comparatively greater reductions in E-selectin (Figure 4B).

Collectively, these results demonstrate that both Beetvaso and Beetvaso-P effectively inhibit HFD-induced endothelial activation and vascular inflammation through down-regulation of VCAM-1, ICAM-1, P-selectin, and E-selectin, suggesting that these extracts mitigate HFD-associated vascular dysfunction by suppressing endothelial inflammatory activation.

3.5 | Beetvaso and Beetvaso-P Increase NO Levels in Rat Aorta

Abnormalities in NO production by the vascular endothelium are a key contributor to endothelial dysfunction and are closely associated with the development of atherosclerosis. As shown in Figure 5A,B, aortic NO levels were reduced approximately 60% in the HFD group relative to CON. Both Beetvaso and Beetvaso-P dose-dependently restored NO bioavailability, with the 200 mg/kg dose of each extract approaching or reaching CON-comparable levels. At equivalent doses, Beetvaso-P consistently produced higher NO recovery than Beetvaso, most notably at 200 mg/kg. These results suggest that Beetvaso and Beetvaso-P effectively ameliorate endothelial dysfunction by restoring endothelial NO bioavailability in the aorta.

3.6 | Beetvaso and Beetvaso-P Improve Endothelial Function in Ex Vivo Rat Aortic Rings

Endothelial integrity of isolated rat aortic rings was functionally verified prior to assessment of vasorelaxation responses. Following phenylephrine-induced precontraction, cumulative administration of acetylcholine (ACh; 10^{-8}–10^{-5} M) induced marked relaxation in a subset of aortic rings, indicating preserved endothelial function; these rings were classified as endothelium-intact [Endo(+)]. In contrast, aortic rings that failed to relax in response to ACh but showed robust relaxation to SNP were considered endothelium-denuded [Endo(−)], reflecting intact smooth muscle responsiveness with loss of endothelial activity. Validation of endothelial integrity based on differential responses to ACh and SNP is presented in Figure S3.

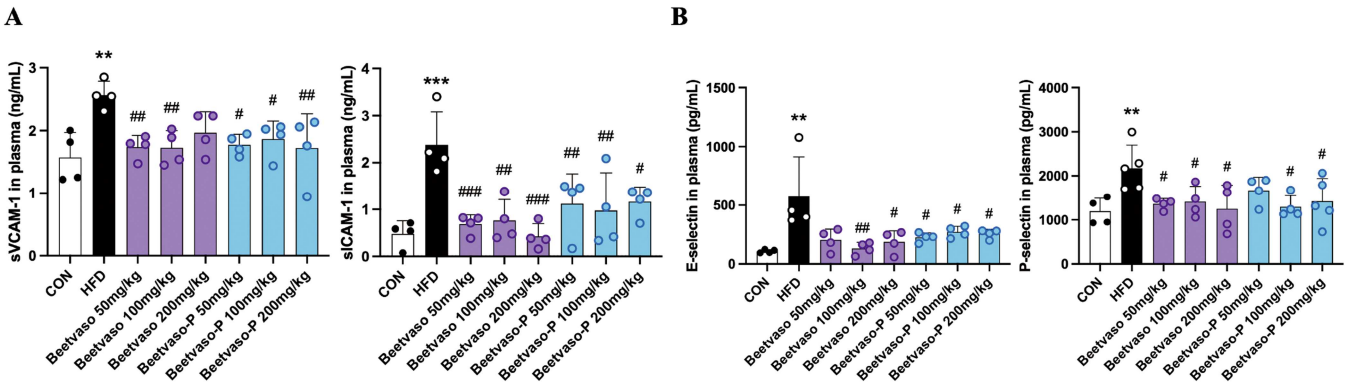


FIGURE 4 | Plasma ELISA analysis of endothelial inflammation and adhesion markers in rats. Soluble adhesion molecules, including (A) soluble VCAM-1 and soluble ICAM-1, and endothelial selectins, including (B) E-selectin and P-selectin. Data are presented as mean ± SD ($n = 4$). Statistical significance is indicated as $^{**}p < 0.01$, $^{***}p < 0.001$, vs. CON; $^{\#}p < 0.05$, $^{\#\#}p < 0.01$, $^{\#\#\#}p < 0.001$ vs. HFD, as annotated in the graphs. Statistical graphs were generated using GraphPad Prism version 10.

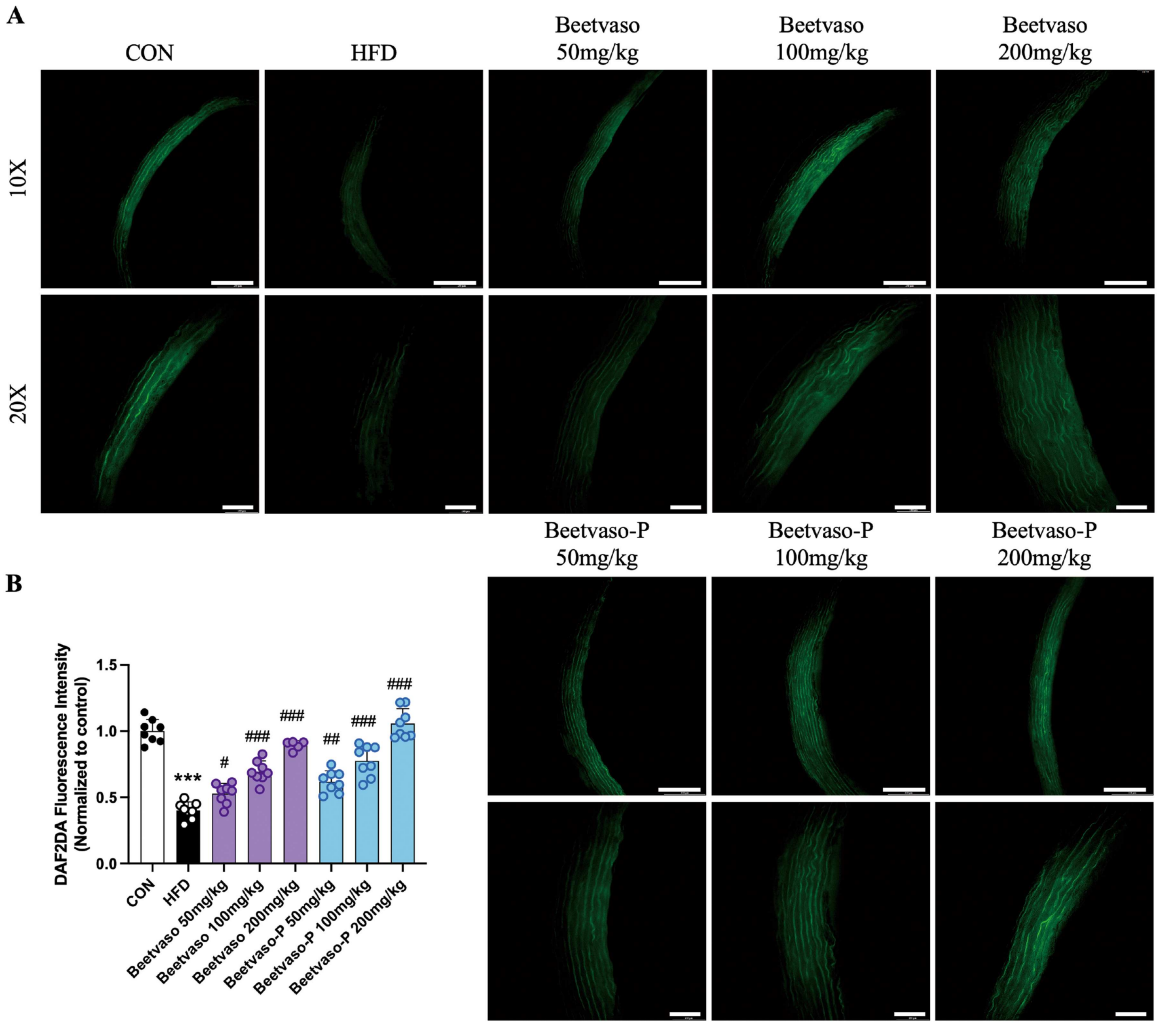


FIGURE 5 | DAF-2DA-based detection of nitric oxide (NO) production in rat aorta. Isolated aortic tissues were incubated with DAF-2DA to visualize NO-dependent fluorescence under microscopy. (A) Representative fluorescence images of aortic rings stained with DAF-2DA, presented at low magnification (10×) and high magnification (20×) to compare NO-associated fluorescence among groups. Scale bars: 250 μm (10×) and 100 μm (20×). (B) Quantitative analysis of DAF-2DA fluorescence intensity, normalized to the control group (control = 1.0). Data are presented as mean ± SD. Statistical significance is indicated as $^{***}p < 0.001$, vs. CON; $^{\#}p < 0.05$, $^{\#\#}p < 0.01$, $^{\#\#\#}p < 0.001$ vs. HFD, as annotated in the graphs ($n = 8$). Statistical graphs were generated using GraphPad Prism version 10.

After confirmation of vascular viability and endothelial status, aortic rings were stably precontracted with phenylephrine (PE, 10^{-6} M), and vasorelaxation responses were evaluated under Endo(+) and Endo(−) conditions. Cumulative treatment with Beetvaso or Beetvaso-P at concentrations ranging from 0.000001% to 0.01% was then performed to assess endothelium-dependent and endothelium-independent relaxation. Beetvaso induced minimal vasorelaxation under Endo(−) conditions, whereas a significant, concentration-dependent relaxation was observed in Endo(+) aortic rings (Figure 6A–C), indicating that its vasorelaxant effect is largely endothelium dependent. Similarly, Beetvaso-P exhibited limited vasorelaxation in Endo(−) rings but produced greater relaxation than Beetvaso under the same conditions. Notably, Beetvaso-P, unlike Beetvaso, elicited measurable vasorelaxation at the low concentration of 0.00001%, at which Beetvaso did not induce a significant response. Under Endo(+) conditions, Beetvaso-P evoked a robust, concentration-dependent vasorelaxation that exceeded that observed with Beetvaso (Figure 6D–F).

3.7 | Beetvaso and Beetvaso-P Enhance eNOS Signaling in Rat Aorta and HUVECs

We next quantified a targeted panel of 10 vascular homeostatic genes by qRT-PCR and summarized group-level expression patterns using multivariate profiling and pathway annotation (Figure 7A and Figure S4). The 10 genes segregated into a pro-inflammatory endothelial activation cluster (*Ccl2, Nox2, Mmp9, Vcam1, Nfkb1*, and *Icam1*) and an endothelial protective homeostasis cluster (*Nos3, Klf2, Abca1*, and *Adipoq*). The activation cluster comprises NF-κB–driven inflammatory, oxidative, and adhesive genes that are known to reduce eNOS expression or promote eNOS uncoupling and thereby limit NO bioavailability, whereas the homeostasis cluster integrates shear-responsive signaling (*Klf2, Nos3*), lipid-handling capacity (*Abca1*), and adipokine-mediated vasoprotection (*Adipoq*) that collectively support eNOS/NO-dependent endothelial stability.

PCA revealed a clear separation of the HFD group from controls, reflecting coordinated upregulation of pro-inflammatory

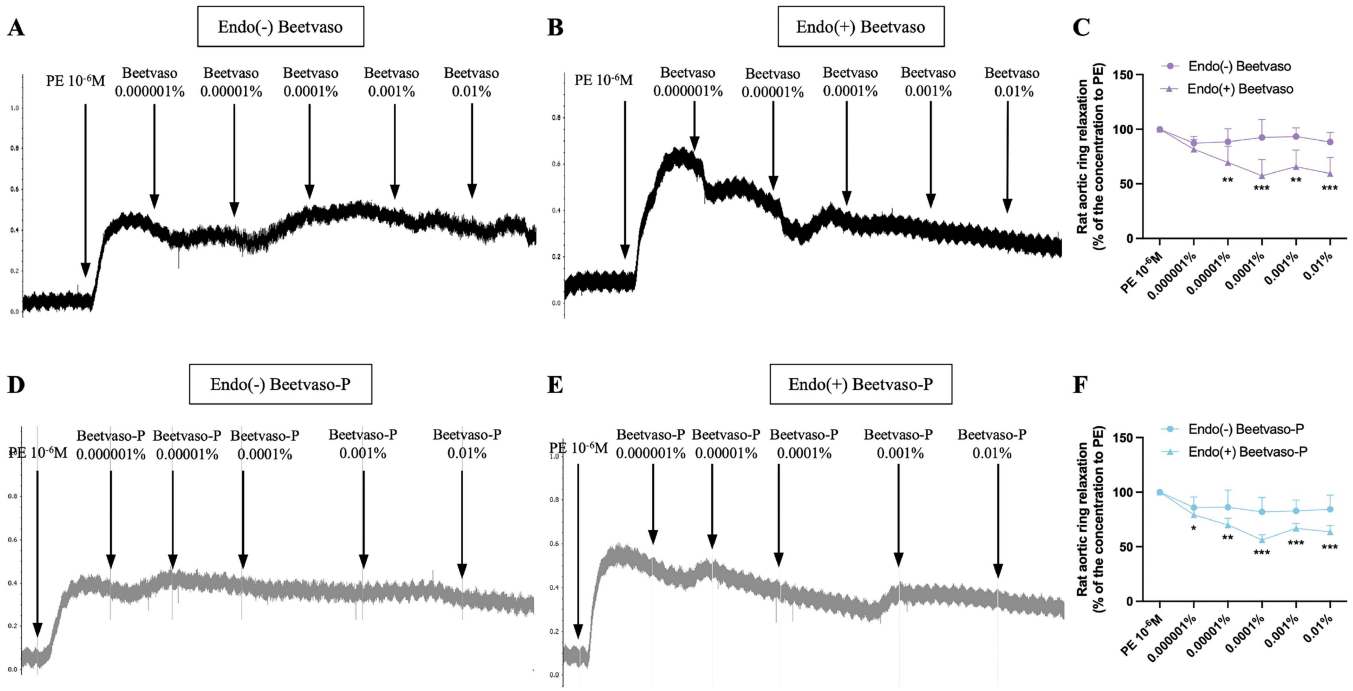


FIGURE 6 | Vasorelaxation responses of isolated rat aortic rings to Beetvaso and Beetvaso-P. Aortic rings were precontracted with phenylephrine (PE, 10^{-6} M), and vasorelaxation responses were evaluated under endothelium-denuded [Endo(−)] or endothelium-intact [Endo(+)] conditions. (A) Representative trace of Beetvaso-induced relaxation in Endo(−) rat aortic rings. (B) Representative trace of Beetvaso-induced relaxation in Endo (+) rat aortic rings. (C) Quantitative analysis of Beetvaso-induced rat aortic ring relaxation, expressed as percentage of relaxation relative to PE-induced contraction. (D) Representative trace of Beetvaso-P–induced relaxation in Endo(−) rat aortic rings. (E) Representative trace of Beetvaso-P–induced relaxation in Endo(+) rat aortic rings. (F) Quantitative analysis of Beetvaso-P–induced rat aortic ring relaxation, expressed as percentage of relaxation relative to PE-induced contraction. Data are presented as mean ± SD ($n = 3$). Statistical significance is indicated as $^{*}p < 0.05$, $^{**}p < 0.01$, $^{***}p < 0.001$ vs. PE (10^{-6} M)-induced baseline contraction. Vasorelaxation traces were recorded and exported using LabChart.

endothelial activation accompanied by downregulation of endothelial protective factors (Figure S4A,B). At the individual gene level, HFD induced robust upregulation across the entire pro-inflammatory cluster relative to CON, with *Nfkb1* showing the greatest induction ($\log_2$FC = 8.74), followed by *Mmp9* (7.17), *Nox2* (6.09), *Icam1* (5.64), *Ccl2* (3.74), and *Vcam1* (2.83; all $p < 0.001$). Conversely, all four homeostasis genes were significantly suppressed, with *Adipoq* and *Abca1* exhibiting the greatest decreases ($\log_2$FC = −7.48 and −6.98), followed by *Klf2* (−4.50) and *Nos3* (−3.07; all $p < 0.001$).

Beetvaso partially attenuated the inflammatory gene cluster, although the overall expression profile remained shifted relative to the control group (Figure 7A and Figure S4A–C). At the highest dose (200 mg/kg), *Mmp9* and *Vcam1* were normalized to CON-comparable levels ($\log_2$FC = −0.14 and 0.85, both ns), *Nos3* expression was restored above CON ($\log_2$FC = 1.09, $p < 0.05$), and *Klf2* and *Abca1* also reached nonsignificant levels ($\log_2$FC = 0.39 and −0.93, both ns), indicating partial rescue of the homeostatic program. In contrast, Beetvaso-P induced a stronger, dose-dependent shift toward a control-like transcriptional pattern. At 200 mg/kg, *Nfkb1* was suppressed well below CON levels ($\log_2$FC = −6.00, $p < 0.001$), accompanied by marked downregulation of its downstream targets *Ccl2* (−16.98, $p < 0.001$), *Mmp9* (−10.47, $p < 0.01$), *Icam1* (−5.68, $p < 0.001$), and *Vcam1* (−4.21, $p < 0.05$). Concurrently, homeostasis genes were substantially upregulated; *Klf2* and *Abca1* were elevated above CON ($\log_2$FC = 5.32 and 3.94, respectively; both $p < 0.001$), and *Nos3* was similarly induced (1.79, $p < 0.01$), indicative of broad restoration of the endothelial protective program.

To directly assess endothelial eNOS signaling, phosphorylation of eNOS at Ser1177 and Thr495 was measured as a readout of eNOS activation. In rat aortic tissue, HFD reduced the p-eNOS (Ser1177)/total eNOS ratio (0.85-fold vs. CON) and the p-eNOS (Ser1177)/p-eNOS(Thr495) ratio (0.73-fold vs. CON), indicating a shift toward an eNOS-inhibitory phosphorylation state. Both extracts dose-dependently reversed this pattern. At 200 mg/kg, Beetvaso increased the p-eNOS(Ser1177)/total eNOS ratio to approximately 2.0-fold above HFD levels and the p-eNOS (Ser1177)/p-eNOS(Thr495) ratio to approximately 3.0-fold. Similarly, Beetvaso-P enhanced the p-eNOS(Ser1177)/total eNOS ratio to approximately 3.0-fold above HFD and the p-eNOS(Ser1177)/p-eNOS(Thr495) ratio to roughly 2.6-fold, consistent with a preferential shift toward the activatory Ser1177 site relative to Thr495 for both extracts (Figure 7B).

Similarly, in HUVECs, TNF-α reduced the p-eNOS(Ser1177)/total eNOS ratio (0.75-fold vs. CON) and the p-eNOS(Ser1177)/p-eNOS(Thr495) ratio (0.72-fold vs. CON). Both Beetvaso and Beetvaso-P concentration-dependently restored these ratios to CON-comparable or above-CON levels at 0.1%, with broadly comparable efficacy between the two extracts (Figure 7C). In addition, both Beetvaso and Beetvaso-P improved endothelial tube formation in TNF-α–treated HUVECs compared with TNF-α alone (Figure S5).

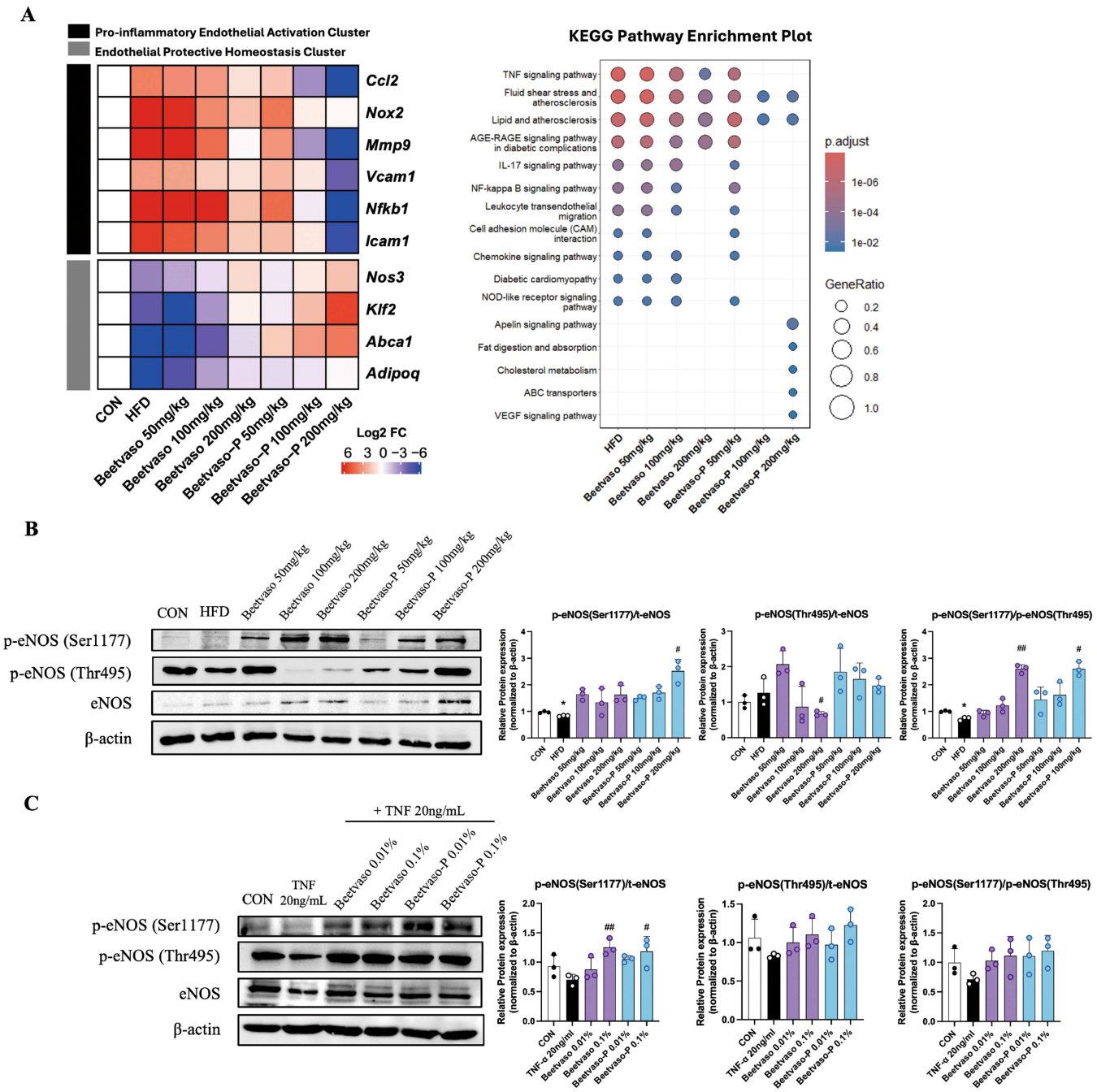


FIGURE 7 | Transcriptional reprogramming and activation of eNOS signaling in rat aorta and HUVECs. (A) Left: Heatmap of targeted qRT-PCR data showing expression of a pro-inflammatory endothelial activation cluster (*Ccl2, Nox2, Mmp9, Vcam1, Nfkb1, Icam1*) and an endothelial-protective homeostasis cluster (*Nos3, Klf2, Abca1, Adipoq*) across experimental groups. Right: KEGG pathway enrichment analysis of differentially expressed genes, displayed as a bubble plot in which dot size represents GeneRatio and color indicates adjusted *p* value. (B) Representative Western blot images (left) and corresponding quantitative densitometric analysis (right) of p-eNOS (Ser1177), p-eNOS (Thr495), total eNOS, normalized to β-actin, in rat aortic tissue. (C) The corresponding analysis was performed in HUVECs. Data are presented as mean ± SD ($n = 3$). Statistical significance is indicated as $^{*}p < 0.05$ vs. CON; $^{\#}p < 0.05$, $^{\#\#}p < 0.01$ vs. HFD or TNF-α, as annotated in the graphs. Statistical graphs were generated using GraphPad Prism version 10.

Taken together, these results indicate that both Beetvaso and Beetvaso-P counteract HFD-induced vascular inflammation by reprogramming NF-κB–driven inflammatory and endothelial homeostasis genes and shifting eNOS phosphorylation toward an activatory state in rat aorta and HUVECs, with Beetvaso-P generally showing greater in vivo efficacy.

4 | Discussion

This study provides integrated evidence that food processing conditions can modulate vascular bioefficacy beyond conventional extraction yield considerations. In an HFD-induced model of endothelial dysfunction, red beet extracts attenuated blood pressure elevation, lipid profiles, endothelial inflammatory activation,

vascular remodeling, and NO–dependent vasorelaxation. Notably, the PEF–treated preparation consistently produced greater structural and molecular normalization than non-PEF–treated preparation, suggesting that upstream processing variables may represent biologically meaningful determinants of endothelial outcomes.

HFD feeding produced a vascular phenotype characterized by systolic hypertension, dyslipidemia, reduced endothelial NO bioavailability, increased adhesion molecule expression, and inward hypertrophic remodeling of the aortic wall. The increase in IMT together with the reduction in lumen area is consistent with early atherosclerosis-like structural alterations. Both extracts attenuated these pathological changes; however, Beetvaso-P more effectively preserved lumen geometry within an unchanged external elastic lamina boundary. This pattern suggests improved structural remodeling rather than passive dimensional expansion. Because endothelial-derived NO plays a central role in regulating vascular tone and structural adaptation, restoration of endothelial signaling likely contributes to this architectural normalization. It should be noted that, while the observed improvements in lumen area and intimal thickness are consistent with active structural reverse remodeling, involving extracellular matrix reorganization and vascular smooth muscle cell phenotype normalization (Z. J. Wang et al. 2023). However, the present study did not directly assess ECM composition or VSMC phenotypic markers. Therefore, the possibility that the observed structural changes reflect passive luminal distension secondary to reduced blood pressure and improved vasodilatory tone cannot be fully excluded.

Functionally, both preparations enhanced endothelium-dependent vasorelaxation and restored NO-associated fluorescence in aortic tissue. These results indicate recovery of endothelial responsiveness under metabolic stress conditions. Importantly, vasorelaxation was predominantly observed in endothelium-intact rings, supporting an endothelial-mediated mechanism rather than direct smooth muscle relaxation. While improved NO bioavailability emerged as a convergent functional endpoint, lipid lowering, inflammatory suppression, and transcriptional normalization likely contributed collectively to this recovery rather than acting through a single linear pathway.

The improvement in coagulation parameters observed following extract treatment further supports the notion of restored endothelial homeostasis. HFD-induced reduction in aPTT indicates a hypercoagulable shift within the intrinsic coagulation pathway, a condition closely linked to endothelial dysfunction and increased thrombotic risk (Lang et al. 2019). Both Beetvaso and Beetvaso-P restored aPTT toward normal levels, suggesting attenuation of this prothrombotic state. The differential effects on vWF and PAI-1 may reflect distinct mechanistic targets of the two extracts. The selective reduction of vWF by Beetvaso is consistent with direct suppression of endothelial activation, as vWF is primarily synthesized and secreted by endothelial cells and is a well-established marker of endothelial dysfunction (Donadini et al. 2025). In contrast, the selective reduction of PAI-1 by Beetvaso-P may be linked to its more pronounced restoration of anti-inflammatory and metabolic gene expression, including *Abca1* and *Adipoq*, together with stronger attenuation of NF-κB-driven transcriptional activation, consistent with the established link between PAI-1 elevation and impaired fibrinolysis (Chen et al. 2017; Morrow and Mutch 2023; Stamatikos et al. 2019). Together, these coagulation-related findings are consistent with a broader restoration of endothelial functional integrity beyond vasomotor regulation alone.

At the molecular level, HFD induced coordinated upregulation of inflammatory and oxidative stress–associated genes alongside downregulation of endothelial-protective regulators. This pattern is consistent with a pro-atherogenic, NF-κB–driven endothelial activation state characterized by enhanced leukocyte recruitment, oxidative stress, and loss of shear-dependent vasoprotective signaling (X. Wang and He 2024). Within this transcriptional context, Beetvaso partially attenuated the HFD-induced shift, whereas Beetvaso-P produced a more coherent reorientation toward a less inflammatory and more vasoprotective, control-like profile. Restoration of key regulators such as *Nos3* and *Klf2* is particularly relevant, as these factors integrate shear-responsive signaling with eNOS/NO-dependent endothelial stability (Tamargo et al. 2024). Recovery of *Abca1* expression may further support improved lipid handling and reduced lipid-driven oxidative stress that impairs NO signaling (Vaisman et al. 2012).

We evaluated two distinct phosphorylation sites on eNOS. Ser1177 is a well-characterized activating site; its phosphorylation by Akt enhances eNOS activity and promotes NO production (Liang et al. 2021). By contrast, Thr495 is classically described as inhibitory; phosphorylation by PKC sterically blocks calmodulin binding and reduces eNOS activity (Fleming et al. 2001). In our HFD model, treatment with both extracts increased phosphorylation at Ser1177 together with a smaller concomitant rise at Thr495, indicating that the overall Ser1177/Thr495 balance was shifted toward eNOS activation. Consistent with this, the magnitude of Ser1177 phosphorylation was greater than that of Thr495, supporting a net shift toward eNOS activation (Matsumoto et al. 2014). In addition, both extracts increased endothelial NO bioavailability in our model, as reflected by elevated DAF-2DA fluorescence in aortic tissue and enhanced endothelium-dependent vasorelaxation in ex vivo aortic rings.

A critical implication of this study is that the enhanced efficacy of the PEF–treated extract cannot be fully explained by a higher concentration of bioactive compounds. Although equivalent doses were administered across all treatment groups, Beetvaso-P produced greater structural and molecular improvements than Beetvaso. This suggests that qualitative differences in composition, rather than quantity alone, may drive the observed effects. PEF pretreatment did not enrich red betacyanins in Beetvaso-P; betanin was no longer detectable and betanidin intensity was slightly reduced, whereas several betaxanthins, including vulgaxanthin I and indicaxanthin, remained relatively preserved. Thus, Beetvaso-P represents a betalain fraction in which the original red–yellow balance is shifted toward a betaxanthin-enriched profile, rather than a simple quantitative increase in total betalains.

Previous studies suggest that betaxanthins and betacyanins exhibit distinct redox and inflammatory modulatory properties. Despite the loss of red betacyanins, Beetvaso-P exerted greater

vascular protective effects in HFD-fed rats compared with conventionally extracted Beetvaso, suggesting that yellow betaxanthins and related metabolites may play a more prominent functional role. In support of this interpretation, indicaxanthin, a betaxanthin preserved in Beetvaso-P, has been shown to protect HUVECs against ox-LDL-induced endothelial dysfunction through NF-κB inhibition at physiologically relevant concentrations (Attanzio et al. 2019). Moreover, a study in Caco-2 intestinal epithelial cells comparing betanin, vulgaxanthin I, and indicaxanthin indicates that all three betalains exert anti-inflammatory and antioxidant effects. Notably, the cellular uptake of the two betaxanthins was higher than that of betanin, indicating more favorable absorption characteristics for yellow pigments (Y. Wang et al. 2022). In a human study, despite high betanin contents in both beetroot juice and food form, betanin was undetectable in plasma after ingestion, demonstrating poor systemic bioavailability (Clifford et al. 2017).

Given that betanin—the dominant pigment in Beetvaso—appears to be largely unavailable systemically, a betaxanthin-enriched composition, as in Beetvaso-P, may exert greater efficacy at the systemic level. This strengthens the central argument of the present study that qualitative composition, rather than quantity alone, is the biologically relevant determinant of vascular efficacy. Therefore, our results support the working hypothesis that PEF-induced re-profiling of beetroot betalains—shifting from a betacyanin-dominant to a relatively betaxanthin-enriched extract—may contribute to the enhanced endothelial bioefficacy of Beetvaso-P, rather than a simple increase in total pigment content. However, this remains a correlative association that should be tested directly by comparing purified betacyanin and betaxanthin fractions, as well as their defined combinations, in HUVECs and in an HFD rat model.

Several additional limitations should be considered. First, all experiments were conducted exclusively in male SD rats, which precludes assessment of sex-dependent differences in vascular responsiveness and metabolic adaptation to HFD. Additionally, the HFD–SD rat model encompasses broad metabolic disturbances, making it difficult to attribute the observed vascular improvements solely to direct endothelial effects of Beetvaso-P. Future studies using spontaneously hypertensive rats would allow more direct assessment of Beetvaso-P on eNOS-NO signaling independent of systemic metabolic confounders. Second, although the enhanced efficacy of Beetvaso-P was attributed to betaxanthin enrichment following PEF treatment, the potential contribution of other co-extracted compounds such as polyphenols was not assessed. Polyphenols are well known to enhance NO bioavailability through eNOS activation and ROS scavenging, and their presence in the extract cannot be excluded as a contributing factor to the observed vascular effects. Furthermore, compositional assessment was limited to relative quantification. Future studies incorporating absolute LC–MS profiling alongside fractionation-based functional assays will be necessary to directly establish causal linkage between processing-induced compositional changes and endothelial outcomes.

Altogether, red beet extracts mitigate HFD-induced endothelial dysfunction through coordinated structural, functional, and transcriptional normalization, with PEF pretreatment conferring enhanced vascular bioefficacy. These findings underscore food processing technology as a biologically relevant variable in functional ingredient performance. Processing conditions should therefore be regarded not merely as determinants of extraction efficiency, but as active modulators of bioactive composition and endothelial functional outcomes.

5 | Conclusion

In conclusion, this study provides compelling evidence that PEF processing redefines the biological quality of red beet extracts, positioning Beetvaso-P as a superior functional formulation for mitigating metabolic vascular dysfunction. Our findings indicate that the enhanced vascular protection conferred by PEF-treated extracts is not solely attributable to extraction yield but is driven by a qualitative compositional shift toward betaxanthin enrichment. This shift enhances endothelial eNOS–NO signaling and promotes a vasoprotective transcriptional profile. By demonstrating consistent efficacy across in vivo structural remodeling, ex vivo vasorelaxation, and in vitro endothelial networking, we highlight that processing technology is a biologically relevant determinant of vascular outcomes. These results offer a strategic foundation for utilizing nonthermal processing to optimize plant-derived bioactives as dietary intervention for cardiovascular complications associated with metabolic stress.

Author Contributions

Eunju Jang: writing – original draft, methodology, investigation, formal analysis, data curation, conceptualization, visualization. **Tae-Baek Lee:** writing – original draft, software, investigation, formal analysis, data curation, visualization. **Lisa Tonini:** investigation, data curation. **Soobin Choi:** investigation, data curation. **YoonA Jeon:** methodology, validation. **Taehyun Kim:** investigation, data curation. **Taeyoung Kang:** resources, writing – review and editing. **Hyuk-Joon Choi:** resources, funding acquisition, writing – review and editing. **Changhwan Ahn:** conceptualization, project administration, supervision, writing – review and editing.

Acknowledgments

This research was financially supported by the Ministry of Small and Medium-sized Enterprises (SMEs) and Startups (MSS), Korea, under the "Regional Specialized Industry Development Plus Program (R&D, S3404552)" supervised by the Korea Technology and Information Promotion Agency for SMEs (TIPA).

Conflicts of Interest

The authors declare no conflicts of interest.

Data Availability Statement

The data that support the findings of this study are available from the corresponding author upon reasonable request.

References

Attanzio, A., A. Frazzitta, R. Busa, L. Tesoriere, M. A. Livrea, and M. Allegra. 2019. "Indicaxanthin From *Opuntia ficus indica* (L. Mill) Inhibits Oxidized LDL-Mediated Human Endothelial Cell Dysfunction Through Inhibition of NF-κB Activation." *Oxidative Medicine and Cellular Longevity* 2019: 3457846. https://doi.org/10.1155/2019/3457846.

Chen, Y., Y. Zheng, L. Liu, et al. 2017. "Adiponectin Inhibits TNF-α-Activated PAI-1 Expression via the cAMP-PKA-AMPK-NF-κB Axis in

Human Umbilical Vein Endothelial Cells." *Cellular Physiology and Biochemistry* 42, no. 6: 2342–2352. https://doi.org/10.1159/000480006.

Clifford, T., C. M. Constantinou, K. M. Keane, D. J. West, G. Howatson, and E. J. Stevenson. 2017. "The Plasma Bioavailability of Nitrate and Betanin From *Beta vulgaris rubra* in Humans." *European Journal of Nutrition* 56, no. 3: 1245–1254. https://doi.org/10.1007/s00394-016-1173-5.

Darvish, S., K. Ludwig, A. Ikoba, et al. 2024. "Nitrate-Rich Beetroot Juice Supplementation in Midlife and Older Adults With Renal Dysfunction Increases Vascular Endothelial Function and Changes the Circulating Milieu to Improve Endothelial Cell Nitric Oxide Production and Oxidative Stress." *Physiology* 39, no. S1: 389. https://doi.org/10.1152/physiol.2024.39.S1.389.

Dobrian, A. D., M. J. Davies, R. L. Prewitt, and T. J. Lauterio. 2000. "Development of Hypertension in a Rat Model of Diet-Induced Obesity." *Hypertension* 35, no. 4: 1009–1015. https://doi.org/10.1161/01.hyp.35.4.1009.

Donadini, M. P., F. Calcaterra, E. Romualdi, et al. 2025. "The Link Between Venous and Arterial Thrombosis: Is There a Role for Endothelial Dysfunction?," *Cells* 14, no. 2: 144. https://doi.org/10.3390/cells14020144.

Fejes, R., N. Pilat, M. Lutnik, et al. 2024. "Effects of Increased Nitrate Intake From Beetroot Juice on Blood Markers of Oxidative Stress and Inflammation in Older Adults With Hypertension." *Free Radical Biology and Medicine* 222: 519–530. https://doi.org/10.1016/j.freeradbiomed.2024.07.004.

Fincan, M., F. DeVito, and P. Dejmek. 2004. "Pulsed Electric Field Treatment for Solid–Liquid Extraction of Red Beetroot Pigment." *Journal of Food Engineering* 64, no. 3: 381–388. https://doi.org/10.1016/j.jfoodeng.2003.11.006.

Fleming, I., B. Fisslthaler, S. Dimmeler, B. E. Kemp, and R. Busse. 2001. "Phosphorylation of Thr495 Regulates Ca^{2+}/Calmodulin-Dependent Endothelial Nitric Oxide Synthase Activity." *Circulation Research* 88, no. 11: e68–e75. https://doi.org/10.1161/hh1101.092677.

García-Prieto, C. F., F. Hernández-Nuño, D. D. Rio, et al. 2015. "High-Fat Diet Induces Endothelial Dysfunction Through a Down-Regulation of the Endothelial AMPK-PI3K-Akt-eNOS Pathway." *Molecular Nutrition & Food Research* 59, no. 3: 520–532. https://doi.org/10.1002/mnfr.201400539.

Higashi, Y. 2022. "Roles of Oxidative Stress and Inflammation in Vascular Endothelial Dysfunction-Related Disease." *Antioxidants* 11, no. 10: 1958. https://doi.org/10.3390/antiox11101958.

Kaya, T., S. Gursoy, B. Karadas, B. Sarac, H. Fafali, and A. S. Soydan. 2003. "High-Concentration Tramadol-Induced Vasodilation in Rabbit Aorta Is Mediated by Both Endothelium-Dependent and -Independent Mechanisms." *Acta Pharmacologica Sinica* 24, no. 5: 385–389. https://www.ncbi.nlm.nih.gov/pubmed/12740170.

Kim, S.-Y., H. L. Gu, H. Ju, J. Jeon, S.-H. Jeong, and D.-U. Lee. 2024. "Effects of Pulsed Electric Fields on Controlling Fermentation Rate of Brined *Raphanus sativus*." *Innovative Food Science & Emerging Technologies* 92: 103553. https://doi.org/10.1016/j.ifset.2023.103553.

Lang, P., S. Hasselwander, H. Li, and N. Xia. 2019. "Effects of Different Diets Used in Diet-Induced Obesity Models on Insulin Resistance and Vascular Dysfunction in C57BL/6 Mice." *Scientific Reports* 9, no. 1: 19556. https://doi.org/10.1038/s41598-019-55987-x.

Liang, X., R. Wang, Y. Guo, et al. 2021. "Phosphorylation of Akt at Thr308 Regulates p-eNOS Ser1177 During Physiological Conditions." *FEBS Open Bio* 11, no. 7: 1953–1964. https://doi.org/10.1002/2211-5463.13194.

Litwin, N. S., H. J. Van Ark, S. C. Hartley, et al. 2019. "Impact of Red Beetroot Juice on Vascular Endothelial Function and Cardiometabolic Responses to a High-Fat Meal in Middle-Aged/Older Adults With Overweight and Obesity: A Randomized, Double-Blind, Placebo-Controlled, Crossover Trial." *Current Developments in Nutrition* 3, no. 11: nzz113. https://doi.org/10.1093/cdn/nzz113.

López, N., E. Puértolas, S. Condón, J. Raso, and I. Alvarez. 2009. "Enhancement of the Extraction of Betanine From Red Beetroot by Pulsed Electric Fields." *Journal of Food Engineering* 90, no. 1: 60–66. https://doi.org/10.1016/j.jfoodeng.2008.06.002.

Luengo, E., J. M. Martinez, I. Álvarez, and J. Raso. 2016. "Comparison of the Efficacy of Pulsed Electric Fields Treatments in the Millisecond and Microsecond Range for the Extraction of Betanine From Red Beetroot." In *1st World Congress on Electroporation and Pulsed Electric Fields in Biology, Medicine and Food & Environmental Technologies*, edited by T. Jarm and P. Springer.

Matsumoto, S., M. Shimabukuro, D. Fukuda, et al. 2014. "Azilsartan, an Angiotensin II Type 1 Receptor Blocker, Restores Endothelial Function by Reducing Vascular Inflammation and by Increasing the Phosphorylation Ratio Ser(1177)/Thr(497) of Endothelial Nitric Oxide Synthase in Diabetic Mice." *Cardiovascular Diabetology* 13: 30. https://doi.org/10.1186/1475-2840-13-30.

Milton-Laskibar, I., J. A. Martínez, and M. P. Portillo. 2021. "Current Knowledge on Beetroot Bioactive Compounds: Role of Nitrate and Betalains in Health and Disease." *Foods* 10, no. 6: 1314. https://doi.org/10.3390/foods10061314.

Morrow, G. B., and N. J. Mutch. 2023. "Past, Present, and Future Perspectives of Plasminogen Activator Inhibitor 1 (PAI-1)." *Seminars in Thrombosis and Hemostasis* 49, no. 3: 305–313. https://doi.org/10.1055/s-0042-1758791.

Stamatikos, A., N. Dronadula, P. Ng, et al. 2019. "ABCA1 Overexpression in Endothelial Cells In Vitro Enhances ApoAI-Mediated Cholesterol Efflux and Decreases Inflammation." *Human Gene Therapy* 30, no. 2: 236–248. https://doi.org/10.1089/hum.2018.120.

Tamargo, I. A., K. I. Baek, C. Xu, et al. 2024. "HEG1 Protects Against Atherosclerosis by Regulating Stable Flow-Induced KLF2/4 Expression in Endothelial Cells." *Circulation* 149, no. 15: 1183–1201. https://doi.org/10.1161/CIRCULATIONAHA.123.064735.

Toque, H. A., A. Fernandez-Flores, R. Mohamed, R. B. Caldwell, G. Ramesh, and R. W. Caldwell. 2017. "Netrin-1 Is a Novel Regulator of Vascular Endothelial Function in Diabetes." *PLoS One* 12, no. 10: e0186734. https://doi.org/10.1371/journal.pone.0186734.

Vaisman, B. L., S. J. Demosky, J. A. Stonik, et al. 2012. "Endothelial Expression of Human ABCA1 in Mice Increases Plasma HDL Cholesterol and Reduces Diet-Induced Atherosclerosis." *Journal of Lipid Research* 53, no. 1: 158–167. https://doi.org/10.1194/jlr.M018713.

Wang, X., and B. He. 2024. "Endothelial Dysfunction: Molecular Mechanisms and Clinical Implications." *MedComm* 5, no. 8: e651. https://doi.org/10.1002/mco2.651.

Wang, Y., G. S. N. Fernando, N. N. Sergeeva, et al. 2022. "Uptake and Immunomodulatory Properties of Betanin, Vulgaxanthin I and Indicaxanthin Towards Caco-2 Intestinal Cells." *Antioxidants* 11, no. 8: 1627. https://doi.org/10.3390/antiox11081627.

Wang, Z. J., Q. W. Guan, H. H. Zhou, X. Y. Mao, and F. H. Chen. 2023. "Mechanistic Insight Into Lysyl Oxidase in Vascular Remodeling and Angiogenesis." *Genes & Diseases* 10, no. 3: 771–785. https://doi.org/10.1016/j.gendis.2022.05.011.

Zhou, D., T. Liu, S. Wang, W. He, W. Qian, and G. Luo. 2020. "Effects of IL-1β and TNF-α on the Expression of P311 in Vascular Endothelial Cells and Wound Healing in Mice." *Frontiers in Physiology* 11: 545008. https://doi.org/10.3389/fphys.2020.545008.

Supporting Information

Additional supporting information can be found online in the Supporting Information section.

Figure S1: Changes in plasma lipid levels in rats fed a high-fat diet and treated with Beetvaso or Beetvaso-P. Rats were fed an HFD for 3 months and subsequently administered Beetvaso or Beetvaso-P (50, 100, or 200 mg/kg) orally for three weeks. Blood samples were collected to

assess major lipid parameters. (A) Levels of total cholesterol (TC) were measured in the plasma of rats in different experimental groups. (B) Triglyceride (TG) levels in plasma. (C) Low-density lipoprotein cholesterol (LDL-C) levels. Data are presented as mean ± SD (n = 4). Statistical significance is indicated as * $p < 0.05$, vs. CON; # $p < 0.05$, ## $p < 0.01$, ### $p < 0.001$ vs. HFD, as annotated in the graphs. Statistical graphs were generated using GraphPad Prism version 10.

Figure S2: Additional morphometric analyses of aortic remodeling. (A) Representative low-magnification images of thoracic aorta cross-sections. Scale bars: 200 μm. (B) External elastic lamina (EEL) area (mm^2). (C) EEL diameter (mm). (D) Lumen-to-EEL area ratio (%). EEL denotes the external elastic lamina, representing the outer vessel boundary used for size-normalized assessment of lumen geometry. Bars indicate group means with individual data points overlaid (each dot represents one animal). Data are presented as mean ± SD ($n = 8$). Statistical significance is indicated as * $p < 0.05$, vs. CON; # $p < 0.05$, ## $p < 0.01$ vs. HFD, as annotated in the graphs. Statistical graphs were generated using GraphPad Prism version 10.

Figure S3: Functional validation of endothelial integrity in isolated rat aortic rings. Endothelial integrity of isolated rat aortic rings was verified based on differential vasorelaxation responses to acetylcholine (ACh) and sodium nitroprusside (SNP) following phenylephrine-induced precontraction. (A) Channel 9: aortic ring exhibiting no relaxation in response to ACh but preserved relaxation to SNP, classified as endothelium-denuded [Endo(−)]. (B) Channel 10: aortic ring showing a similar response pattern, with absence of ACh-induced relaxation and intact SNP-induced relaxation, classified as Endo(−). (C) Channel 11: aortic ring displaying marked relaxation in response to ACh, indicating preserved endothelial function, classified as endothelium-intact [Endo (+)]. (D) Channel 12: aortic ring exhibiting robust ACh-induced relaxation, confirming intact endothelium [Endo(+)]. These functional criteria were used to distinguish endothelium-intact and endothelium-denuded aortic rings prior to the assessment of vasorelaxation responses to Beetvaso and Beetvaso-P. Vasorelaxation traces were recorded and exported using LabChart.

Figure S4: Multivariate analysis of HFD–induced transcriptional dysregulation and its modulation by Beetvaso and Beetvaso-P. (A) Principal component analysis (PCA) of the targeted aortic qRT-PCR gene expression panel across experimental groups. Each point represents an individual sample, and group clustering is shown in the PC1–PC2 space, with the explained variance indicated on each axis. (B) Volcano plots summarizing gene-level responses for the HFD group and each treatment group. The x-axis indicates log2 fold change, and the y-axis indicates −log (FDR); dashed lines denote the predefined effect size and significance thresholds. Genes are colored by significance category (significantly upregulated, significantly downregulated, or not significant), and representative endpoints are annotated. (C) Rescue plots assessing normalization of HFD–induced transcriptional changes by Beetvaso and Beetvaso-P at each dose. The x-axis denotes disease induction defined as log2FC (HFD − CON), and the y-axis denotes rescue effect defined as log2FC (Treatment − HFD). Points near the negative diagonal indicate stronger reversal toward the control direction, whereas deviations indicate partial or non-rescue patterns.

Figure S5: Beetvaso and Beetvaso-P restore endothelial tube formation in TNF-α–treated HUVECs. Human umbilical vein endothelial cells (HUVECs) were treated with TNF-α in the absence or presence of Beetvaso or Beetvaso-P, and endothelial tube formation was quantified. (A) Representative brightfield images (left) and corresponding ImageJ-processed images (right) of tube formation in HUVECs treated with TNF-α and Beetvaso or Beetvaso-P. (B) Quantitative analysis of tube formation parameters, including junction number, mesh number, and total tube length, in HUVECs treated with TNF-α and Beetvaso or Beetvaso-P. Data are presented as mean ± SD ($n = 4$). # $p < 0.05$ vs. TNF-α–treated group. Statistical graphs were generated using GraphPad Prism version 10.